



Regular Article

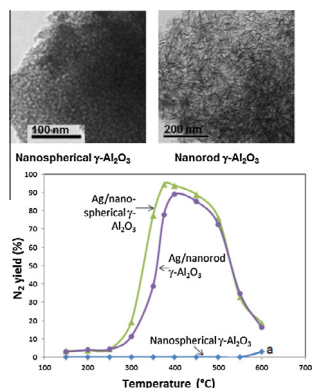
A new route to the shape-controlled synthesis of nano-sized γ -alumina and Ag/ γ -alumina for selective catalytic reduction of NO in the presence of propene



Driss Mrabet, Manh-Hiep Vu, Serge Kaliaguine*, Trong-On Do*

Department of Chemical Engineering, Laval University, Quebec G1V 0A6, Canada

GRAPHICAL ABSTRACT



ARTICLE INFO

Article history:

Received 26 August 2016

Accepted 10 September 2016

Available online 15 September 2016

Keywords:

γ -Nanoalumina

Nanocrystals

γ -Nanoalumina based Ag catalysts

Selective catalytic reduction

NO

C_3H_6

ABSTRACT

We report a new route for the direct synthesis of γ -alumina nanocrystals with size and shape control in the presence of oleylamine as the capping agent. Their morphology can be controlled from nanospheres to nanorods by simply tuning a proper amount of concentrated nitric acid (67%) in the synthetic mixture. The as-made nanoparticle products after calcination show γ -alumina nano-size with unique porosity and high specific surface area and retained morphology. The XRD patterns of these calcined samples exhibit broad diffraction lines which are characteristic of nanocrystal size of γ -alumina.

This synthesis procedure has been extended to the one-pot synthesis of nano-alumina based Ag catalysts with spherical and rod-shaped nano-alumina morphologies. Selective catalytic reduction (SCR) of NO with C_3H_6 over these catalysts was investigated. The results were compared to those of the conventional Ag/ γ - Al_2O_3 and γ -nanoalumina alone. These nano-alumina based Ag catalysts exhibit excellent NO reduction activity in the presence of C_3H_6 . Even in the presence of large oxygen concentration (15%), N_2 yields as high as $\sim 90\%$ at quite low temperature (~ 350 $^\circ\text{C}$) have been achieved. The significantly high catalytic activity of this new type of nanocatalysts can also be attributed to their high surface area and good dispersion of silver species in the alumina matrix as well as the synergism and new properties that arise at the silver-nanoalumina interface.

© 2016 Elsevier Inc. All rights reserved.

1. Introduction

The size- and shape of nanoparticles (NPs) and their self-assembly have significant effect on their performances in

* Corresponding authors.

E-mail addresses: serge.kaliaguine@gch.ulaval.ca (S. Kaliaguine), Trong-On.Do@gch.ulaval.ca (T.-O. Do).

application as catalysts. The NPs exhibit size-dependent characteristics and novel properties that cannot be achieved using their bulk counterparts [1–5]. Controlling the shape of oxide particles on the nanoscale enriches their active sites (i.e., their electronic structure and surface coordination environment) through the selective exposure of reactive facets on their surface, which improves the catalytic performance [6–9]. A variety of NPs types with desired sizes and shapes have been developed for specific applications including nanospheres, nanotubes, nanorods and nanosheets [2,6,10,11].

The self-assembly of mono-disperse NPs into three-dimensional ordered super-structures has rapidly attracted a growing interest due to the surface of nanocrystals inherently rich in coordinately unsaturated sites that can play an important role in catalytic reactions. Among all metal oxides, γ -alumina nanocrystals are particularly important, because they are widely used as an electrical insulator, fillers for nanocomposites, adsorbents, catalysts and catalytic support, owing to their high thermal stability and low cost. Because of their broad range of applications, the development of simple synthetic methods including high yield, shape-controlled nanocrystals and anisotropic nanorods under mild conditions is of key importance [10–13].

Three-dimensional ordered nanostructure assembled from metal and metal oxide NPs could also provide better catalytic performance over conventional catalysts, due to new properties that arise at the metal/metal oxide interface. In addition, a nanosupport such as nano-sized γ -alumina does not act as an inert carrier but intervenes in the catalytic reactions [2,3,12]. The alumina shape was also found to alter the chemical states of supported metal nanoparticles under reaction conditions. Defect sites with coordinately unsaturated Al^{3+} in the alumina particles usually form the binding sites that anchor the metal nanoparticles or clusters. A prominent example is the pentacoordinated Al^{3+} sites on the (100) facets of γ -alumina, which preferentially anchored Pt nanoparticles to form highly dispersed Pt species [14,15]. A significant shape effect of ZnO nanoparticles on the interaction with copper for the formation of methanol by hydrogenation of CO_2 was also reported by Liao et al. [10,11].

The particle size effect has typically been explained on the basis of variations in the number of active sites; small particles with high surface-to-volume ratios offer more active sites consisting of low-coordinated atoms in defect sites such as terraces, edges, kinks, or vacancies [1–4]. Increasing evidence now suggests that the shape of the catalyst particle is equally important for obtaining the desired catalytic activity and selectivity [2–5,10]. This morphological dependence becomes more significant with decreasing size along specific dimensions. Only a few examples of this type of porous metal-metal oxide particles are yet known. The development of simple approaches for the synthesis of this type of materials is therefore important and still remains challenging [16–18].

In this study, we report a new route for the one-pot nonhydrolytic synthesis of γ -alumina nanocrystals with size and shape control in the presence of oleylamine as the capping agent. The morphology of alumina nanoparticles (from spherical to rod-shaped nanocrystals) can be easily tuned using proper amounts of concentrated nitric acid (67%) added in the synthetic mixture. These nanoparticle products after calcination show γ -alumina nanophase with unique porosity and specific surface area and however retained their morphology. This procedure was also extended to the synthesis of nano Ag/ γ -alumina catalysts. NO reduction in the presence of propene and excess oxygen (15%) over the obtained nano-Ag/ γ -alumina nanocatalysts is also demonstrated and compared with that observed on the conventional Ag/ γ - Al_2O_3 catalyst.

2. Experimental

2.1. Preparation of materials

Chemicals: All chemicals were of analytical grade and used without further purification. Oleylamine (70%), toluene, aluminum isopropoxide (98%), nitric acid (HNO_3 67%), were purchased from Sigma-Aldrich.

For the synthesis of nano-sized alumina with different morphologies, typically, 0.75 g (3.7 mmol) aluminum isopropoxide was added to 50 ml of toluene containing 1.4 g (5.2 mmol) of oleylamine. After complete dissolution, to this mixture, an appropriated amount of nitric acid (67%) is added. The mixture was stirred vigorously for 1 h at room temperature, then sealed in a Teflon-lined stainless-steel autoclave of 80 ml capacity and heated at 180 °C for 20 h. The autoclave was then cooled down to room temperature. The nanocomposite products were precipitated with an excess ethanol and further isolated by centrifugation. The resulting solid products were dried at 105 °C and calcined at 600 °C for 4 h under air flow. For the synthesis of Ag/nano-sized alumina, the same procedure was applied; however, 0.02 g (0.01 mmol) of silver nitrate was added in the synthetic mixture. *For comparison*, the conventional 2.0 wt% Ag/ γ - Al_2O_3 sample was also prepared by impregnation using commercial γ - Al_2O_3 powders as support (Alfa products, SA: 200 m^2/g) with an appropriate amount of silver nitrate aqueous solution, at room temperature for 6 h, then dried at 100 °C overnight, and finally calcined under air flow at 600 °C for 4 h.

2.2. Characterisation of materials

BET surface area, pore volume and pore diameter: BET surface area of the calcined samples were obtained from N_2 adsorption/desorption isotherms measured at -196 °C using an automated gas sorption system (NOVA 2000, Quantachrome) operating in continuous mode. The specific surface area was determined from the linear part of the BET curve ($P/P_0 = 0.01–0.15$). Pore volume and average diameter were obtained from pore size distribution curve, which was calculated from the desorption branch of N_2 adsorption/desorption isotherms using the Barret-Joyner-Halenda (BJH) formula. **Transmission Electron Microscopy (TEM):** Particle size and morphology of the materials were studied using transmission electron microscopy (TEM). TEM images were obtained on a JEOL JEM 1230 Transmission Electron Microscope operating at 120 kV. The nanocomposite materials were dispersed in toluene and cast onto a 200 mesh carbon-coated copper grid sample followed by evaporation at room temperature. **X-ray Powder Diffraction (XRD):** XRD patterns were recorded using a Siemens D 5000 X-ray diffractometer using filtered $\text{Cu K}\alpha$ ($\lambda = 1.54062$ Å) radiation (40 kV, 30 mA). The data were collected over a 2θ range of 20–80° with a scan step of 0.02° and an acquisition time of 1.2 s per step. The crystal phases are identified using the JCPDS. **Temperature-Programmed Reduction (TPR):** Prior to H_2 -TPR, the sample (50 mg) was pretreated under a 10% O_2/He flow at 20 cm^3/min total flow rate (STP) for 1 h at 550 °C; cooled down to room temperature under the same atmosphere; purged with 20 cm^3/min total flow at 5% H_2/Ar , and streamed with a rising temperature of up to 900 °C at a constant heating rate of 5 °C/min. The water in the effluent gas of the TPR process was condensed via a cold trap with a mixture of dry-ice and ethanol. H_2 consumption was monitored continuously by TCD using a flow of 20 cm^3/min of 5% H_2/Ar as a reference gas. The gas responses obtained by MS and TCD during transient studies were calibrated using standard mixtures.

2.3. Catalytic activity

Catalytic tests were performed under steady-state conditions in a quartz tube fixed-bed reactor [13,19,20]. The system was heated externally via a tubular furnace, regulated by a temperature controller (Omega CN3240) via a thermocouple in contact with the catalyst bed, to raise the reactor temperature by steps of 50 °C from 150 °C to 600 °C. A feed gas with 1000 ppm NO, 3000 ppm C₃H₆ and 15% oxygen with helium as a balance was fed to 50 mg of catalyst at a total flow rate of 60 ml/min, which corresponded to a 28,000 h⁻¹ space velocity. N₂ and O₂ in the reactor effluent were analysed using a HP 5890A gas chromatograph equipped with a molecular sieve column combined with a silicone column using a TCD detector. The effluent gases (C₃H₆, CO₂, H₂O, NO₂, CO) were monitored using an Infrared analyzer (FT-IR) model (FTLA 2000, ABB). The NO conversion and NO₂ yield were determined using a chemi-luminescence NO/NO₂/NO_x analyzer (model 200AH, Advanced Pollution Instrumentation (API), USA).

3. Results and discussion

3.1. γ -Nanoalumina with shape control

Reliable information about the effect of nitric acid amount on the morphology of nano-alumina, the crystalline phase as well as the mesopore structure can be obtained from transmission electron micrograph (TEM) images, XRD patterns and from nitrogen adsorption/desorption experiments. Table 1 summarizes the synthetic conditions and the physico-chemical properties of a series of samples obtained with varying nitric acid amounts (denoted as Nano-alumina[x], where x is the volume in ml of HNO₃ 67% added in the synthetic mixture). This series of nanoalumina samples were prepared by varying the amount of nitric acid (67%) from 0 to 5 ml, while keeping other parameters unchanged: the amount of aluminum isopropoxide, AIP (0.75 g or 3.7 mmol), oleylamine, OA (1.4 g or 5.2 mmol), and the volume of toluene (50 ml).

Fig. 1 shows representative TEM images of the samples prepared with different amounts of HNO₃ 67% (from 0 to 5 ml) after calcination at 600 °C for 4 h. It is seen that the morphology varies from spherical to rod-shaped nanocrystals depending on nitric acid quantity added in the synthesis mixture. It is important to note that no significant change in morphology of these samples was observed after calcination. When in the absence or the presence of only 1 ml of 67% nitric acid (the volume ratio of 1/50) was added, spherical-shaped alumina NPs with uniform size are obtained (Fig. 1a, b). By increasing the amount of 67% nitric acid to 3 ml, a mixture of spherical particles and rod-like particles was observed (Fig. 1c). Closer TEM observation on numerous parts of the sample exhibited that each “nanorod-like” is composed of several nanoparticles; however, nanoparticles were still the exclusive products. This suggests that the larger nanoparticles grow

involving the Ostwald ripening rather than the oriented attachment during this synthesis. Furthermore, when nitric acid amount was increased to 5 ml, no spherical nanoparticles were essentially found; concomitantly, only individual nanorods along the common axis with ~5 nm width and 80–100 nm length were formed. This indicates a complete transformation from nanoparticles to nanorods. One can also point out that, in this case, no change in width of nanoparticles was observed and the alumina NPs remained monodisperse in size.

An analysis of the particle size evolution as a function of nitric acid amount using TEM shows that the nanocrystal growth involves two mechanisms: coarsening well-known as Ostwald ripening and oriented attachment. Nanoparticles were formed at 180 °C by consuming aluminum isopropoxide precursors in the absence or the presence of only small quantity of nitric acid (<3 ml). With the increase of nitric acid amount (up to 5 ml) in the synthetic mixture, because no aluminum isopropoxide precursors were added during the synthesis, the aluminum precursor concentration in the bulk solution is very low; with a sufficient amount of nitric acid-water, spherical nanocrystals can rearrange to find the lower-energy configuration by a coherent particle-particle interface. Therefore, nanorods could be formed, due to the oriented attachment process [21,22].

Fig. 2 shows the XRD patterns of the as-made samples with different amounts of nitric acid added in the synthetic solution, before and after calcination at 600 °C for 4 h. For the as-made samples, the alumina phase depends on the nitric acid concentration in the synthetic mixture. Without nitric acid, only amorphous phase was essentially observed, even after calcination (Fig. 2A, a). Interestingly, when only minor amounts of nitric acid (67%) were added (1 and 2 ml) in the synthetic mixture, broad diffraction peaks which are characteristic of γ -Al₂O₃ phase (JCPDS No. card 29-0063) were achieved. These peaks at around 2 θ = 38.0, 46.0 and 66.1° correspond to the (3 1 1), (4 0 0) and (4 4 0) reflections, respectively (Fig. 2A, b-c). The reflection broadness suggests the formation of nanocrystalline domains in the sample. However, with increasing nitric acid amount (to 3.0 ml), two predominant alumina phases of γ - and boehmite phases were observed (Fig. 2A, d). At higher nitric acid amount (to 5.0 ml), the sample shows typical peaks of the boehmite phase before calcination (JCPDS card No. 05-0190) (Fig. 2A, f).

The formation of boehmite is due the presence of sufficient water in the synthetic mixture which accelerates the hydrolysis of aluminum isopropoxide and the condensation at high temperature and thus leads to the formation of aluminum oxyhydroxide instead of aluminum oxide [13]. This also indicates that the γ -Al₂O₃ phase formed at the early stage was transformed to boehmite during the synthesis, with increasing nitric acid amount (e.g., an increase of water contained in nitric acid 67%). However, after calcination at 600 °C in air, all the samples exhibit γ -Al₂O₃ phase, except for the sample prepared in the absence of nitric acid,

Table 1

Synthesis conditions and textural properties before and after calcination of the nano-alumina samples prepared with different amounts of nitric acid.

Sample	HNO ₃ 67% (ml)	Phase		S _{BET} (m ² /g)	Pore diameter (nm)	Pore volume (cm ³ /g)
		Before calcination	After calcination			
Nano-alumina-0	0	Amorphous	Amorphous	440	NA	NA
Nano-alumina-0.5	0.5	γ -Al ₂ O ₃	γ -Al ₂ O ₃	371	3.5	0.38
Nano-alumina -1	1	γ -Al ₂ O ₃	γ -Al ₂ O ₃	362	3.6	0.38
Nano-alumina-2	2	γ -Al ₂ O ₃ + boehmite	γ -Al ₂ O ₃	351	50	0.52
Nano-alumina-3	3	γ -Al ₂ O ₃ + boehmite	γ -Al ₂ O ₃	372	10.1	1.27
Nano-alumina-5	5	Boehmite	γ -Al ₂ O ₃	298	14.0	1.21

Nano-alumina-x: where x is the volume in ml of HNO₃ 67%.

Synthesis conditions: (i) aluminum isopropoxide: 3.7 mmol, (ii) toluene: 50 ml, (iii) oleylamine: 5.2 mmol, (iv) nitric acid 67%: 0–5 ml. The mixture sealed in a Teflon-lined stainless-steel autoclave and heated at 180 °C for 20 h.

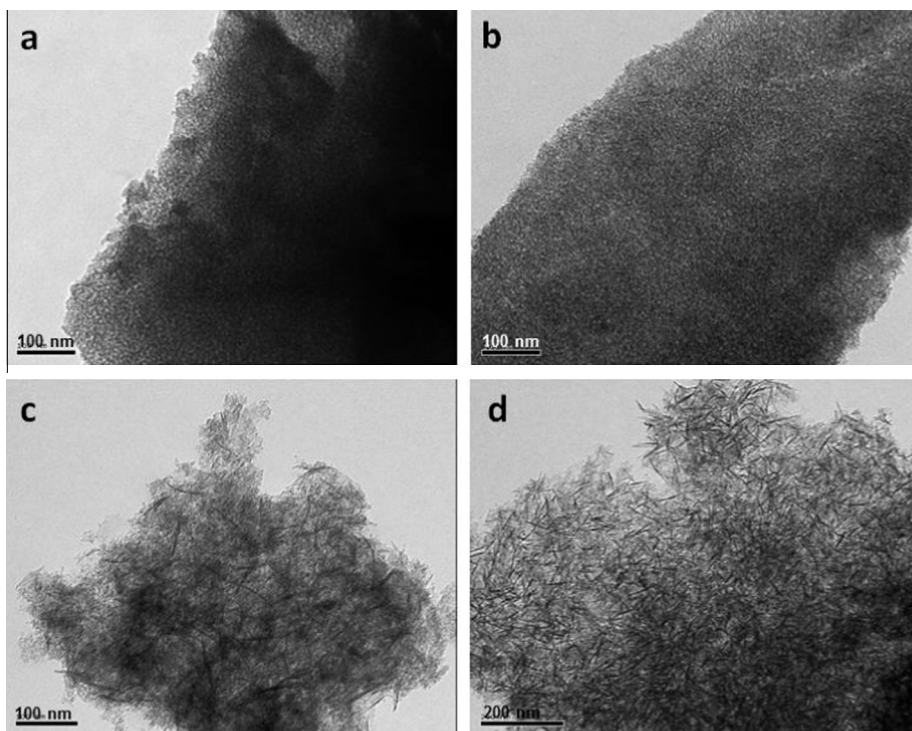


Fig. 1. TEM images of the nano-alumina samples prepared with various amounts of concentrated nitric acid (67%) after calcination at 600 °C for 4 h: (a) 0.5, (b) 1 ml, (c) 3 ml and (d) 5 ml of nitric acid 67%.

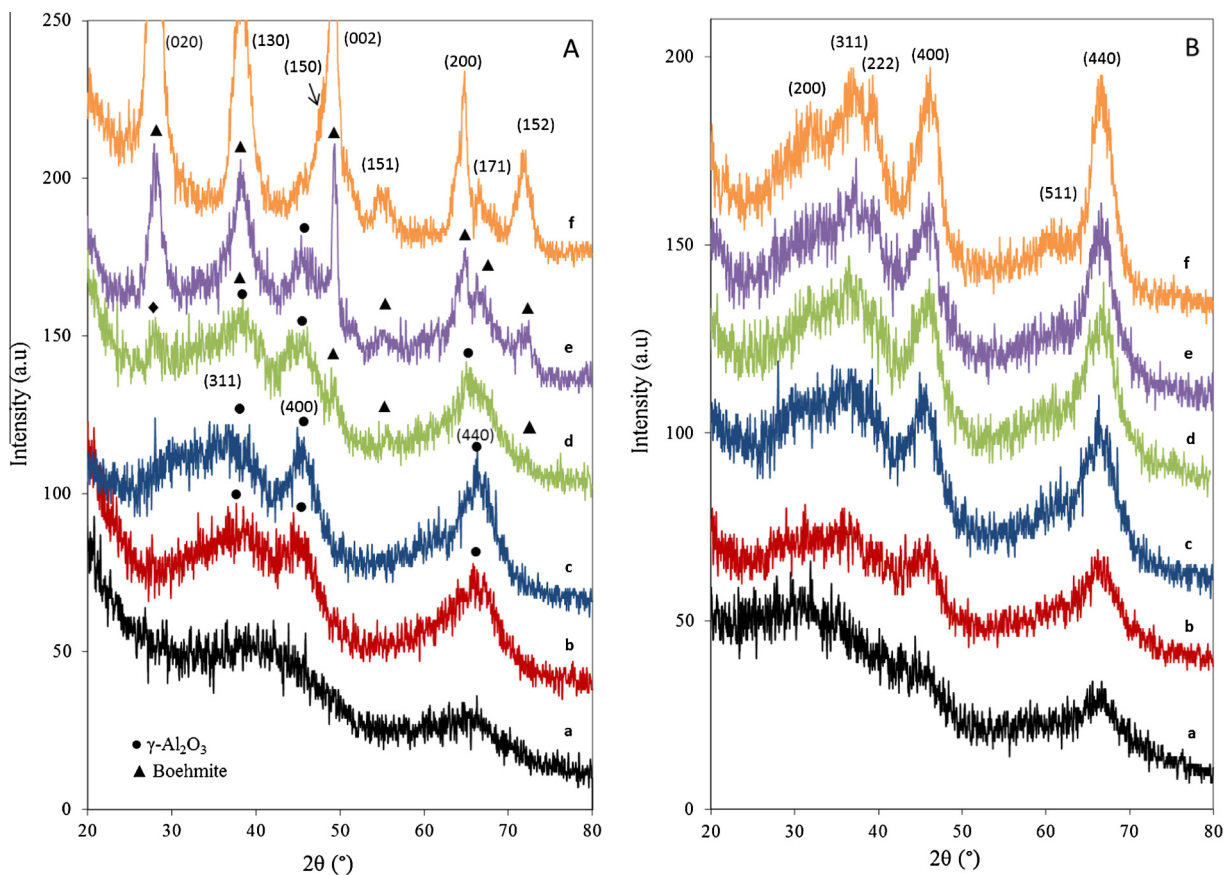


Fig. 2. XRD patterns of the nano-alumina samples prepared avec various amounts of concentrated nitric acid 67% (denoted as Nano-Al-x: where x is the volume in ml of HNO₃ 67%): (A) before and (B) after calcination at 600 °C in air for 4 h. (a) 0 ml, (b), 0.5 ml (c), 1 ml (d), 2 ml (e), 3 ml and (f) 5 ml of nitric acid 67%.

because no peaks corresponding to γ - Al_2O_3 phase was observed for this calcined sample, and an amorphous phase was essentially found (Fig. 2B). For all samples prepared in the presence of nitric acid (67%) after calcination at 600 °C, broad peaks characteristic of γ - Al_2O_3 phase were observed indicating the formation of γ - Al_2O_3 nanocrystals. Furthermore, these peaks are more intense indicating higher γ - Al_2O_3 crystallinity with increasing nitric acid amount. It is important to note that the morphology of these samples did not change essentially, even after calcination at 600 °C for 4 h.

BET specific surface area, pore volume and average pore diameter of this series of calcined samples with different nitric acid amounts are summarized in Table 1. Nitrogen adsorption/desorption isotherms and the corresponding BJH pore size distribution (inset) of the calcined samples are shown in Fig. 3. All samples display classical type IV isotherms with H_1 hysteresis loops, which is typical for mesoporous materials [23]. As seen in Fig. 3, the capillary condensation step is shifted to higher relative pressures with increasing nitric acid amount (from 0 to 5.0 ml), indicating larger mesopores.

For the Nano-Al samples prepared without and with a small amount of nitric acid 67% (0.5 and 1.0 ml), nitrogen adsorption/desorption isotherms exhibit a H_1 hysteresis loop and steep rises at relatively low P/P_0 pressure indicating small pore diameter. Furthermore, high specific surface area of 440 and 371 and 362 m^2/g were achieved for Nano-Al-0, Nano-Al-0.5 and Nano-Al-1.0

samples, respectively. This suggests that the samples prepared by our one step method have a relatively high specific surface area. With increasing nitric acid amount (to 2, 3 and 5 ml), nitrogen adsorption/desorption isotherms of these samples exhibit similar inflection, but shifted toward higher P/P_0 values. A significant increase in pore diameter and pore volume as well as a broader pore-size distribution with increasing nitric acid amount was observed (Fig. 3-inset), whereas the specific surface area of these samples decreased from 440 to 298 m^2/g . As shown in Table 1, the decrease in specific surface area and the increase in pore volume with nitric acid amount could be related to the change in morphology of nano-alumina from nanospheres to nanorods, according to the TEM observation (Fig. 1).

3.2. Ag/ γ -nanoalumina catalysts and catalytic activity

The same procedure was used for the one-pot synthesis of Ag/nanoalumina catalysts (denoted as nano-Ag/alumina-x), except that silver nitrate was added as the silver source in the synthetic mixture. Two nano-Ag/alumina-x catalysts containing ~2 wt% Ag were prepared by using 1.0 and 5.0 ml of nitric acid, respectively ($x = 1$ and 5 ml). NO reduction in the presence of propene over the obtained nano-Ag/alumina catalysts after calcination was investigated and compared with that over the conventional Ag/ γ - Al_2O_3 catalyst. Their activities were evaluated under the

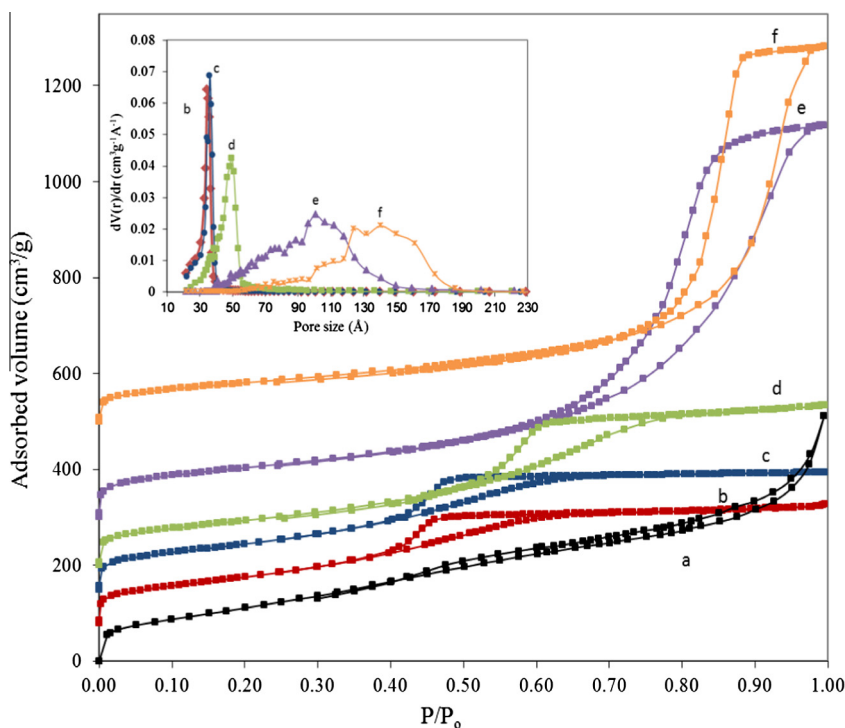


Fig. 3. N_2 adsorption/desorption isotherms of the nano-alumina samples after calcination at 600 °C for 4 h (inset: pore diameter distributions): where x = 0 ml (a), 0.5 ml (b), 1 ml (c), 2 ml (d), 3 ml (e), 5 ml (f) of nitric acid 67% (see Table 1).

Table 2

Textural properties of the calcined nano-Ag/alumina samples (denoted as Nano-Ag/alumina-x: where x is the volume in ml of HNO_3 67%).

Sample	HNO_3 67% (ml)	Ag loading (%)	Phase after calcination	S_{BET} (m^2/g)	Pore diameter (nm)	Pore volume (cm^3/g)
Nano-Ag/alumina-1.0	1	2.2	γ - Al_2O_3	400	3.5	0.38
Nano-Ag/alumina-5.0	5	2.0	γ - Al_2O_3	310	12.5	1.12
Ag/commercial γ - Al_2O_3	–	2.5	γ - Al_2O_3	195	–	–
Nano-alumina-1	1	0	γ - Al_2O_3	362	3.6	0.38

condition of 1000 ppm NO, 2600 ppm C₃H₆, 15% O₂, GHSV: 28,000 h⁻¹ [13].

The physico-chemical properties of these samples are summarized in Table 2. TEM images of these calcined samples are shown in Fig. 4. Spherical-shaped alumina NPs with uniform size were observed for nano-Ag/alumina-1.0; however, “nanorod-like” alumina NPs with ~5 nm width and 80–100 nm length were displayed for nano-Ag/alumina-5.0. Average Ag nanoparticle diameter is found to be 5–8 nm for both samples. Fig. 5 shows the nitrogen adsorption isotherms of the calcined nano-Ag/ γ -alumina samples prepared by adding 1.0 and 5.0 ml of nitric acid, respectively. Again, nitrogen adsorption/desorption isotherms of these

two samples show type IV with H₁ hysteresis loops characteristic of mesoporous materials. For nano-Ag/ γ -alumina-1.0, the isotherms exhibit steep capillary condensation steps which indicate uniform mesopores with the pores diameter of ~3.5 nm; however, the condensation step for the latter sample is shifted to higher relative pressures, indicating larger mesopore diameter and higher pore volume, as shown in Fig. 5-inset and Table 2.

The XRD powder patterns of these two calcined nano-Ag/ γ -alumina samples, shown in Fig. 6A also display three distinct reflections at $2\theta = 38, 46$ and 66° , which corresponds to the standard for γ -Al₂O₃ nanoparticles (JCPDS No. 29-1486). The broad reflections indicate the formation of nanocrystalline alumina

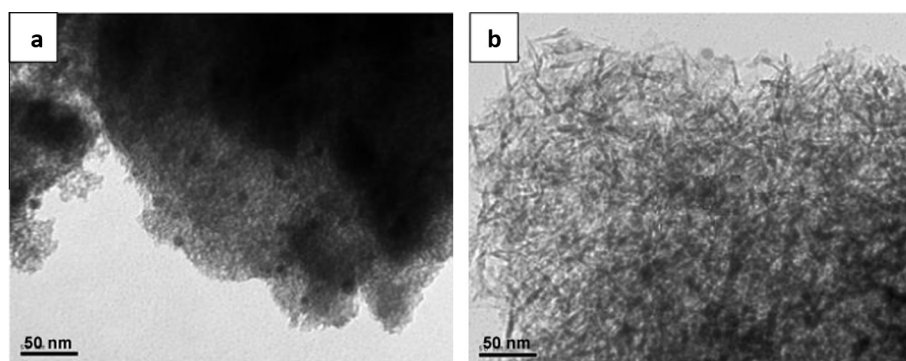


Fig. 4. TEM images of the samples of Ag/ γ -nano-alumina prepared with (a) 1 ml, and (b) 5 ml of nitric acid 67% after calcination at 600 °C for 4 h.

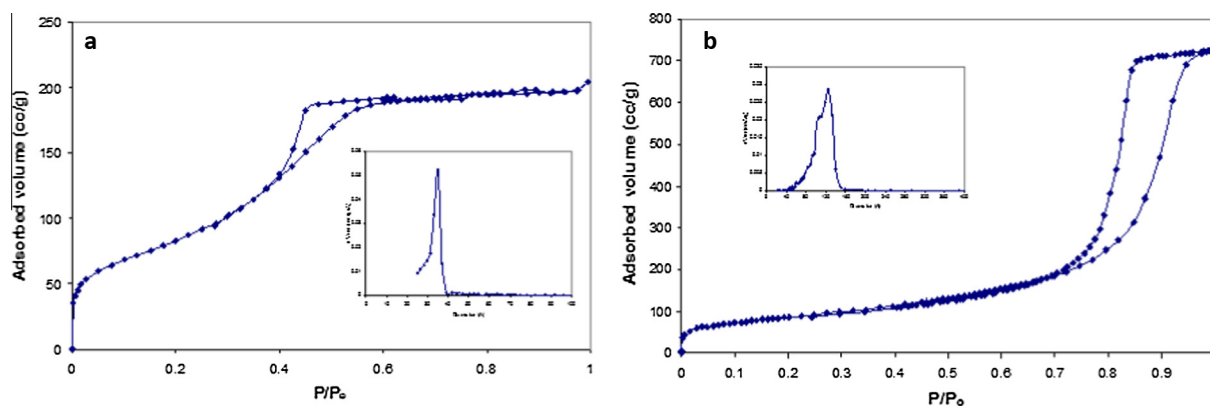


Fig. 5. N₂ adsorption/desorption isotherms of the samples of Ag/ γ -nano-alumina prepared with (a) 1 ml, and (b) 5 ml of nitric acid 67% after calcination at 600 °C for 4 h (inset: pore diameter distribution).

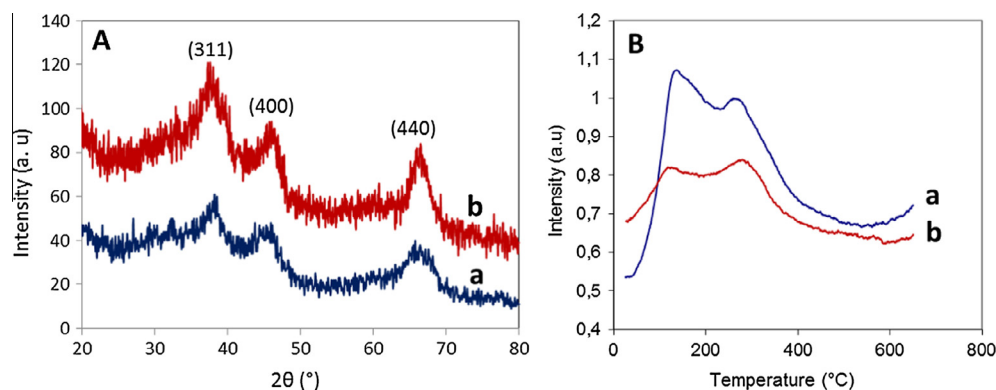


Fig. 6. XRD patterns (A) and H₂-temperature-programmed reduction profiles (B) of the calcined samples of Ag/ γ -nano-alumina prepared with (a) 1 ml, and (b) 5 ml of nitric acid 67%.

domain in the sample even after calcination at 600 °C for 4 h suggesting the high thermal stability of the nanocrystals. No XRD peak characteristic of silver oxide was visible, indicating the high dispersion and small particle size of silver oxide on the alumina support. As silver species did not react with alumina, the high dispersion and Ag loading led also to increase in catalyst surface area and stability, due to suppression of grain growth and sintering [3,6,24]. The nanocomposites containing ~2.0 wt% Ag have BET surface areas of 400 and 310 m²/g for nano-Ag/alumina-1.0 and nano-Ag/alumina-5.0, respectively (Table 2). The reducibility of silver oxide in these calcined samples was also studied by H₂-temperature-programmed reduction (H₂-TPR). The reduction profiles of the calcined samples are shown in Fig. 6B. Both samples exhibit two broad reduction peaks at relatively low temperature (100–400 °C). The temperature reduction peak at ~160 °C was likely ascribed to the reduction of fine Ag₂O particles. However, the second broad reduction peak at higher temperature could be due to the strongly interacting isolated silver oxide species with the alumina support and their high dispersion in the alumina matrix.

The NO reduction activities of these two nano-Ag/ γ -alumina catalysts compared with those of the conventional Ag/ γ -Al₂O₃ and nano-alumina alone samples in the presence of high concentration oxygen (15% O₂) are shown in Figs. 7A–7D. The nano-Ag/alumina-1.0 catalyst exhibits the highest N₂ yield of 95% at 350 °C, which is slightly better than the N₂ yield of ~85% from the nano-Ag/alumina-5.0 sample. The yields of these two catalysts were much higher than that of the conventional Ag/ γ -Al₂O₃ catalyst. Only 60% of N₂ yield at higher temperature (~400 °C) was achieved for this conventional Ag/ γ -Al₂O₃. In the case of the nano-alumina-1 alone, no catalytic activity was found. Fig. 7B shows the NO conversion over these catalysts. The NO conversion curves were similar to N₂ yield curves for these silver catalysts, reflecting the high selectivity toward N₂ during SCR reaction. For nano-Ag/ γ -alumina-1.0 and nano-Ag/ γ -alumina-5.0, the NO conversion passed through a maximum of 90% and 85% at 350 °C, and then declined down to 75% and 68% at 500 °C, respectively; a low NO conversion of 60% was observed for the conventional Ag/ γ -Al₂O₃ catalyst at 400 °C and kept essentially unchanged up to 500 °C.

The high catalytic activity is attributed to the high specific surface area, nanosized alumina and high dispersion of silver nanoparticles in these two nano-Ag/ γ -alumina catalysts compared to those of the conventional Ag/ γ -Al₂O₃ catalyst. As shown in Table 2, the BET specific surface areas of these nano-Ag/ γ -alumina-1.0,

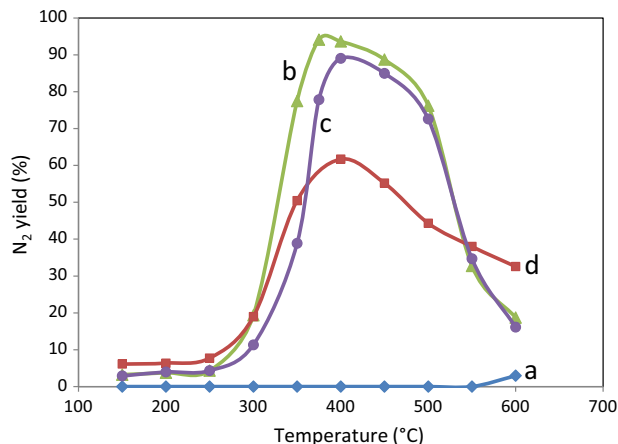


Fig. 7A. N₂ yield in selective catalytic reduction of NO with C₃H₆ over different alumina-based catalysts: (a) γ -nanoalumina; (b) nano-Ag/ γ -nanoalumina-1.0; (c) nano-Ag/ γ -alumina-5.0; (d) conventional Ag/ γ -alumina. Catalytic test conditions: 1000 ppm NO, 2600 ppm C₃H₆, 15% O₂, GHSV: 28,000 h⁻¹.

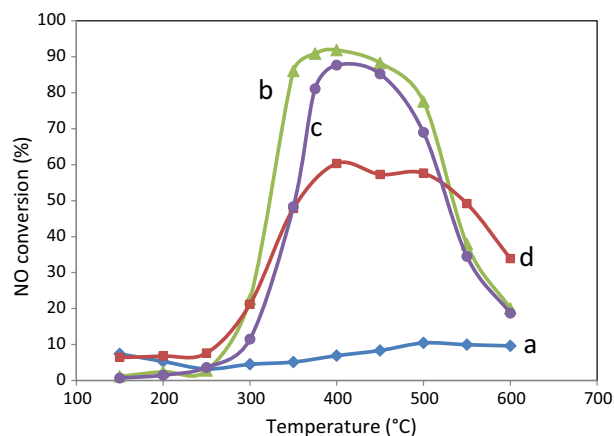


Fig. 7B. NO conversion in selective catalytic reduction of NO with C₃H₆ over different alumina-based catalysts: (a) γ -nanoalumina; (b) nano-Ag/ γ -nanoalumina-1.0; (c) nano-Ag/ γ -alumina-5.0; (d) conventional Ag/ γ -alumina. Catalytic test conditions: 1000 ppm NO, 2600 ppm C₃H₆, 15% O₂, GHSV: 28,000 h⁻¹.

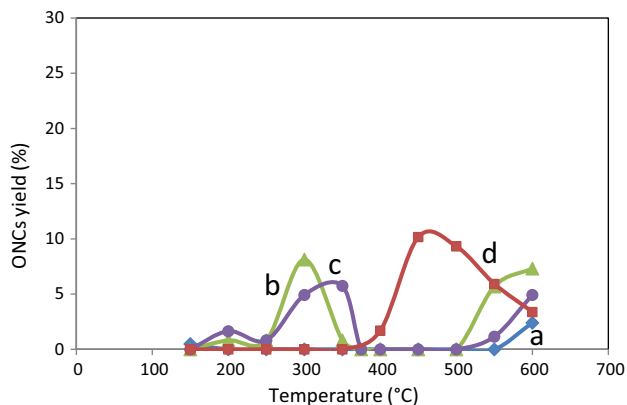


Fig. 7C. ONCs yield in selective catalytic reduction of NO with C₃H₆ over different alumina-based catalysts: (a) γ -nanoalumina; (b) nano-Ag/ γ -nanoalumina-1.0; (c) nano-Ag/ γ -alumina-5.0; (d) conventional Ag/ γ -alumina.

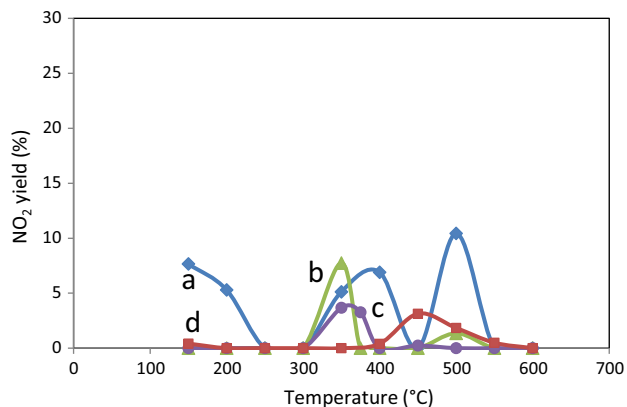


Fig. 7D. NO₂ yield in selective catalytic reduction of NO with C₃H₆ over different alumina-based catalysts: (a) γ -nanoalumina; (b) nano-Ag/ γ -nanoalumina-1.0; (c) nano-Ag/ γ -alumina-5.0; (d) conventional Ag/ γ -alumina.

nano-Ag/ γ -alumina-5.0 and conventional Ag/ γ -Al₂O₃ are 400, 310 and 195 m²/g, respectively. As indicative (Fig. 7C), a small amount of organo-nitrogen compounds (ONCs) at 200–400 °C was also detectable, due to the partial conversion of NO in the effluent

and showed yields in the following order: nano-Ag/ γ -alumina-1.0 > nano-Ag/ γ -alumina-5.0 > conventional Ag/ γ -Al₂O₃ \gg γ nano-alumina. The obvious ONCs yields over conventional Ag/ γ -Al₂O₃ and nano-Ag/ γ -alumina-1.0 at >400 °C have maxima at ~10% and ~5%, respectively. NO₂, another nitrogen containing by-product was also found, as illustrated in Fig. 7D.

It is known that for a catalyst to be effective, it must be able to activate the propene molecule, as well as adsorb NO_x on its surface [24–29]. The synergism between the active component (e.g., silver nanoparticle) and nanocrystalline alumina could enhance the activated propene species and improved NO adsorption on the catalyst surface, which is utilized in the reduction of NO to N₂. The remarkable NO_x activity of our nanocomposites arose in part from the high dispersion of silver species and high specific surface area. However, synergistic effects at the interface of metal nanoparticle/metal oxide nano-support could be likely the origin of the high catalytic activity [11,12].

4. Conclusions

In summary, nanocrystalline γ -alumina with size and shape control from nano-spheres to nano-rods can be directly synthesized by tuning proper amounts of concentrated nitric acid (~67%) with oleylamine as the capping agent. These nanocrystalline γ -alumina samples show very high specific surface area, which varies from 440 to 298 m²/g, depending on the nitric acid amount added in the synthetic mixture.

This synthesis approach was extended for the direct synthesis of nano-Ag/nano-alumina catalysts with spherical and rod-shaped nano-alumina morphology by using 1.0 and 5.0 ml of nitric acid (67%). The two catalysts prepared by this method exhibit excellent NO reduction activity, due to their high surface area and good dispersion of silver species in the alumina matrix. N₂ yields as high as ~95 and ~85% at quite low temperature (at ~350 °C), even in the presence of large oxygen concentration (15%) were achieved over nano-Ag/ γ -alumina-1.0 and nano-Ag/ γ -alumina-5.0, respectively. The significantly improved activity could be attributed to the formation of heterojunctions between nanosilver and nanoalumina and their synergetic interaction that arises at the silver/alumina interface. The catalytic behavior of the catalysts with different silver loadings and silver nanoparticle

size will be investigated [30]. A fundamental understanding of active sites in morphologically tunable oxides enclosed by the desired shapes, which is expected to direct the development of highly efficient nanocatalysts is in progress in our laboratories.

References

- [1] T.D. Nguyen, C.-T. Dinh, T.-O. Do, Chem. Commun. 51 (2015) 624–635.
- [2] Y. Li, W. Shen, Chem. Soc. Rev. 43 (2014) 1543–1574.
- [3] D. Mrabet, M.H. Zahedi-Niaki, T.-O. Do, J. Phys. Chem. C 112 (2008) 7124–7129.
- [4] T.D. Nguyen, C.T. Dinh, T.-O. Do, ACS Nano 4 (2010) 2263–2273.
- [5] C.T. Dinh, T.D. Nguyen, F. Kleitz, T.O. Do, ACS Nano 11 (2009) 3737–3743.
- [6] C.T. Dinh, T.D. Nguyen, F. Kleitz, T.-O. Do, ACS Appl. Mater. Interfaces 3 (2011) 2228–2234.
- [7] R.S. Devan, R.A. Patil, J.H. Lin, Y.R. Ma, Adv. Funct. Mater. 22 (2012) 3326–3370.
- [8] Y. Li, X.Y. Yang, Y. Feng, Z.Y. Yuan, B.L. Su, Solid State Mater. Sci. 37 (2012) 1–74.
- [9] M.J.S. Spencer, Prog. Mater. Sci. 57 (2012) 437–486.
- [10] S. Zhou, M. Antonietti, M. Niederberger, Small 3 (2007) 763–767.
- [11] F. Liao, Z. Zeng, C. Eley, Q. Lu, X. Hong, S.C.E. Tsang, Angew. Chem. Int. Ed. 51 (2012) 5832–5836.
- [12] S. Carrettin, P. Concepcion, A. Corma, J.M.L. Nieto, V.F. Puntes, Angew. Chem., Int. Ed. 43 (2004) 2538–2540.
- [13] R. Zhang, S. Kaliaguine, Appl. Catal. B 78 (2008) 275–287.
- [14] J.H. Kwak, J. Hu, D. Mei, C.W. Yi, D.H. Kim, C.H.F. Peden, L.F. Allard, J. Szanyi, Science 325 (2009) 1670–1673.
- [15] J.H. Kwak, D. Mei, C.W. Yi, D.H. Kim, C.H.F. Peden, L.F. Allard, J. Szanyi, J. Catal. 261 (2009) 17–22.
- [16] C.-T. Dinh, Y. Hoang, F. Kleitz, T.-O. Do, Angew. Chem. Int. Ed. Engl. 53 (2014) 6618–6623.
- [17] C.-C. Nguyen, N.-N. Vu, T.-O. Do, J. Mater. Chem. A 7 (2015) 18345–18359.
- [18] M. Reza Gholipour, C.-T. Dinh, F. B eland, T.-O. Do, Nanoscale 7 (2015) 8187–8208.
- [19] R.D. Zhang, A. Villanueva, H. Alamdari, S. Kaliaguine, J. Catal. 237 (2006) 368–380.
- [20] R.D. Zhang, A. Villanueva, H. Alamdari, S. Kaliaguine, Appl. Catal. B 64 (2006) 220–233.
- [21] T.D. Nguyen, D. Mrabet, T.-O. Do, J. Phys. Chem. C 112 (2008) 15226–15235.
- [22] T.D. Nguyen, T.-O. Do, J. Phys. Chem. C 113 (2009) 11204–11214.
- [23] S.J. Gregg, K.S.W. Sing, Adsorption, Surface Area and Porosity, Academic Press, London, 1982.
- [24] P. Pitukmanorom, J.Y. Ying, Nanotoday 4 (2009) 220–226.
- [25] K. Shimizu, H. Kawabata, A. Satsuma, T. Hattori, J. Phys. Chem. B 103 (1999) 5240–5245.
- [26] F.C. Meunier, J.P. Breen, V. Zuzaniuk, M. Olsson, J.R.H. Ross, J. Catal. 187 (1999) 493–505.
- [27] Y. Chi, S.S.C. Chuang, J. Catal. 190 (2000) 75–91.
- [28] T. Maunula, J. Ahola, H. Hamada, Appl. Catal. B: Environ. 26 (2000) 173–185.
- [29] P.W. Park, S.C. Ragle, C.L. Boyer, M.L. Balmer, M. Engelhard, D. McCready, J. Catal. 210 (2002) 97–105.
- [30] V.I. P arvulescu, B. Cojocar, V. P arvulescu, R. Richards, Z. Li, C. Cadigan, P. Granger, P. Miquel, C. Hardacre, J. Catal. 272 (2010) 92–100.